Consideration of the Maglev Guideway Irregularities in 3-D Dynamics Simulation

Jong-Boo Han, Hyung-Suk Han, Ki-Jung Kim and Chang-Hyun Kimm
Korea Institute of Machinery and Meterials Dept. of Magnetic Levitation and Linear Drive, Daejeon 305-343, KOREA
jbhan@kimm.re.kr, hshan@kimm.re.kr, kkj74@kimm.re.kr, chkim78@kimm.re.kr

ABSTRACT: In the dynamic simulation of Maglev trains in 3-D, it is needed to consider all the guideway irregularities from construction and operation. The determination of the air gap and its velocity both on tangent and curve is derived based on multibody dynamics. Ride and curve negotiation analysis is carried out considering guideway irregularities. The proposed model could be used to establish the tolerances of Maglev guideway geometry.

1 INTRODUCTION

EMS-type urban Maglev vehicles should maintain the levitation within an allowable range of air gap in order to run without touching the guideway. Figure 1 shows Maglev under running test at KIMM' test track. Generally, irregularities of guideway are generated by manufacture and construction tolerance, as well as by thermal deformation. Though such irregularities of a guideway might influence the curving negotiation and ride quality of Maglev vehicles, there has been a lack of research considering the irregularities of curved guideway. Therefore, to evaluate accurately curve negotiation performances of the Maglev vehicle, dynamic analysis for considering irregularities is needed. The goal of this study is to predict curve negotiation performances through a dynamic simulation considering the irregularities of a curved guideway. Since the proposed model is based on 3-dimensional multibody dynamics as shown in Figure 2, it enables more realistic simulation.

Figure 1. Maglev vehicle running over an elevated guideway

2 MODELING

2.1 Vehicle

For the simulation, the model of Maglev vehicle is created in a normal manner in the multibody dynamics field. The Maglev vehicle consists of 2 side frame, 4 anti-roll beams, 2 linear induction motors, 4 air spring, and 2 traction rods.

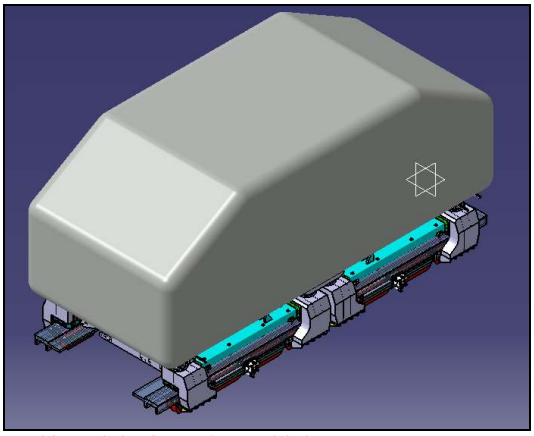

Figure2. Half model of Maglev vehicle

2.2 Electromagnet

A reasonably accurate linear model may be obtained by using linear approximations of the idle levitation force around the nominal equilibrium point (i_0, c_0). Using these linear approximations, the changes in the levitation force and the current are expressed as Equations 1 and 2.

$$F(\Delta c(t), \Delta i(t)) = k_c \Delta c(t) - k_i \Delta i(t) \tag{1}$$

$$\Delta \dot{i}(t) = \frac{k_c}{k_i} \Delta \dot{c}(t) - \frac{R}{L_0} \Delta i(t) + \frac{1}{L_0} \Delta v(t) \tag{2}$$

where,

$L_0 = \dfrac{\mu_0 N^2 A}{2c_0}$

$k_i = \dfrac{\mu_0 N^2 A i_0}{2c_0^{\,2}}$

$k_c = \dfrac{\mu_0 N^2 A i_0^{\,2}}{2c_0^{\,3}}$

F : *Levitation force,*
i_0 : *Nominal current (A),*
A : *Section area of magnet (m^2),*
μ_0 : *Permeability factor,*
c_0 : *Nominal air gap (m),*
c : *Air gap (m),*
v : *Voltage (V),*
R : *Resistance (Ω),*
N : *Number of turn of magnet coil (turn).*

If the lateral air gap of the electromagnet from the guiderail is represented by $d(t) \neq 0$, then the levitation and guidance forces may be expressed as Equation 3 and 4. Here, F_y is vertical force, F_z is guidance force.

$$F_y = F_0 \times \left[-\frac{2c(t)}{\pi \omega_m} \tan^{-1}\left(\frac{c(t)}{d(t)} \right) \right] \tag{3}$$

$$F_z = F_0 \times \left[1 + \frac{2c(t)}{\pi \omega_m} + \frac{2d(t)}{\pi \omega_m} \tan^{-1}\left(\frac{c(t)}{d(t)} \right) \right] \tag{4}$$

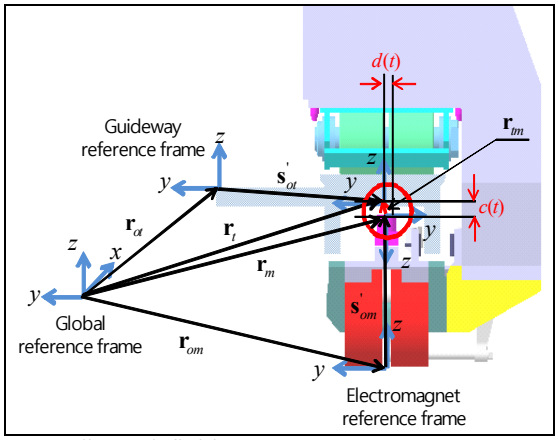

Figure3. Coordinate definition

To apply the electromagnet force using Equation 1~ 4, the $c(t)$, $d(t)$, and $\dot{c}(t)$ can be calculated. Figure 3 shows the definition of vector to calculate the airgaps $(c(t), d(t))$ between the track and the electromagnet. Consequently, the vector between the electromagnet and the guiderail is defined in the global reference frame as

$$\mathbf{r}_{tm} = \mathbf{r}_t - \mathbf{r}_m = \mathbf{r}_{ot} + \mathbf{A}_t \mathbf{s}'_{ot} - \mathbf{r}_{om} - \mathbf{A}_m \mathbf{s}'_{om} \tag{5}$$

Transforming the vector in Equation 5 into the guideway reference frame, the vector in the guideway reference frame is obtained by

$$\mathbf{r}'_{tm} = \begin{bmatrix} x'_{tm}(t) \\ d(t) \\ c(t) \end{bmatrix} = \mathbf{A}_t^T \mathbf{r}_{tm} \tag{6}$$

Here, y component of vector $\mathbf{r}'_{tm}$ is lateral air gap $d(t)$, and z component is vertical air gap $c(t)$.

Differentiating of the vector in Equation 5 and 6 with respect to time, the velocity of air gap $\dot{c}(t)$ can be derived as

$$\begin{aligned} \dot{\mathbf{r}}_{tm} &= \dot{\mathbf{r}}_t - \dot{\mathbf{r}}_m = \dot{\mathbf{r}}_{ot} + \dot{\mathbf{A}}_t \mathbf{s}'_{ot} - \dot{\mathbf{r}}_{om} - \dot{\mathbf{A}}_m \mathbf{s}'_{om} \\ &= \dot{\mathbf{r}}_{ot} + \mathbf{A}_t \tilde{\boldsymbol{\omega}}'_t \mathbf{s}'_{ot} - \dot{\mathbf{r}}_{om} - \mathbf{A}_m \tilde{\boldsymbol{\omega}}'_m \mathbf{s}'_{om} \end{aligned} \tag{6}$$

$$\dot{\mathbf{r}}_{tm}^{'} = \begin{bmatrix} \dot{x}_{tm}^{'}(t) \\ \dot{d}(t) \\ \dot{c}(t) \end{bmatrix} = \mathbf{A}_t^T \dot{\mathbf{r}}_{tm} \tag{7}$$

2.3 Irregularities

Figure 4 shows the guideway static irregularity profile which is represented as the summation of the guideway deflection and surface roughness. It is generated numerically by selecting from a random number generation algorithm. To apply the irregularities, the spline interpolation method is used.

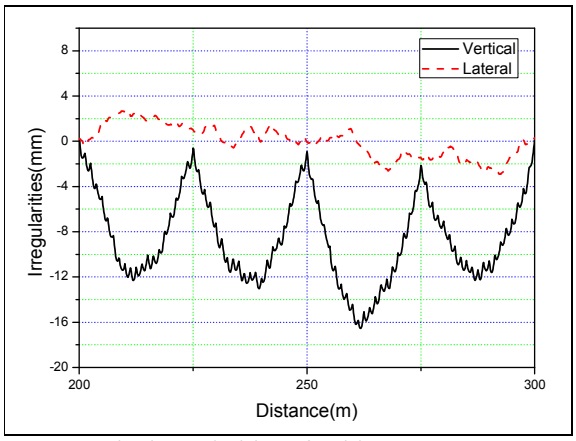

Figure4. Composite irregularities of guideway

Using spline interpolation method, each spline function is obtained as $f_y(x)$ and $f_z(x)$. Those spline functions are calculated each step about longitudinal (x) as shown in Equation 8 and 9.

$$\mathbf{r}_{tm}^{'} = \begin{bmatrix} x_{tm}^{'}(t) \\ d(t) \\ c(t) \end{bmatrix} = \mathbf{A}_t^T \mathbf{r}_{tm} = \mathbf{A}_t^T (\mathbf{r}_t - \mathbf{r}_m)$$

where, (8)

$$\mathbf{r}_t = \mathbf{r}_{ot} + \mathbf{A}_t \mathbf{s}_{tm}^{'} + \mathbf{A}_t \begin{bmatrix} 0 & f_y(s) & f_z(s) \end{bmatrix}^T$$

$$\dot{\mathbf{r}}_{tm}^{'} = \begin{bmatrix} \dot{x}_{tm}^{'}(t) \\ \dot{d}(t) \\ \dot{c}(t) \end{bmatrix} = \mathbf{A}_t^T \dot{\mathbf{r}}_{tm} = \mathbf{A}_t^T (\dot{\mathbf{r}}_t - \dot{\mathbf{r}}_m)$$

where, (9)

$$\dot{\mathbf{r}}_t = \dot{\mathbf{r}}_{ot} + \mathbf{A}_t \tilde{\boldsymbol{\omega}}_t \mathbf{s}_{tm}^{'} + \mathbf{A}_t \tilde{\boldsymbol{\omega}}_t \begin{bmatrix} 0 & \dot{f}_y(s) & \dot{f}_z(s) \end{bmatrix}^T$$

2.4 Curved guideway

A curved guideway is composed of tangent, clothoid curve, and circular curve section. The minimum length of the transition curve is mainly limited by the allowed superelevation gradient, which is determined by the mechanical decoupling tolerance. In this paper, two cases of curved guideway are selected for simulation as shown in Table 1. Firstly, the 35m-length clothoid transition segment and 2.58 cant angle is arranged for the 180m-radius curve at the speed of 30km/h. secondly, the 60m-length clothoid transition segment and 48 cant angle is arranged for the 800m-radius curve at the speed of 80km/h. Based on the above-mentioned curved guideway, the simulation for curving performance is carried out.

Table 1 Simulation conditions

Specification	Case 1	Case 2
Vehicle velocity (km/h)	30	80
Linear section (m)	130	370
Clothoid curve (m)	30	60
Circular curve radius(m)	180	800
Cant (deg)	3	4

2.5 Definition of track coordinate

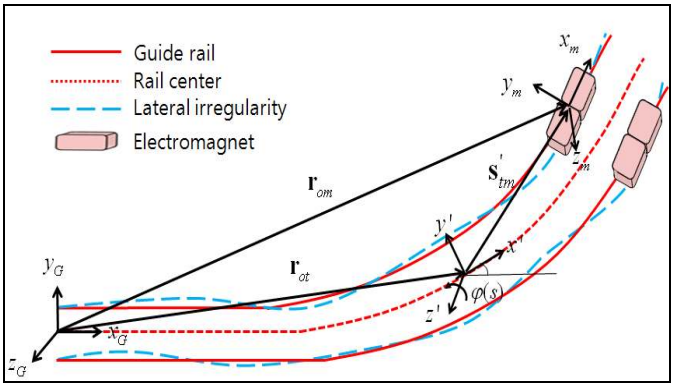

Figure5. Track coordinate

Global vector $\mathbf{r}_t$ consists of vector $\mathbf{r}_{ot}$ and transformation matrix $\mathbf{A}_t$. Also vector of each electromagnet center is able to express $\mathbf{r}_{om}$ and $\mathbf{A}_m$. If coordinate of track center rotates as figure 4, orientation matrix is calculated as Equation 10. Here, $\varphi(x)$ is the rotation angle from the vertical axis, $\beta(x)$ means the angle of the cant between both rails. And orientation matrix of electromagnet is defined using an Euler parameter as Equation 11.

$$\mathbf{A}_t = \begin{bmatrix} 1 & 0 & 0 \\ 0 & \cos(\beta) & -\sin(\beta) \\ 0 & \sin(\beta) & \cos(\beta) \end{bmatrix} \begin{bmatrix} \cos(\varphi) & -\sin(\varphi) & 0 \\ \sin(\varphi) & \cos(\varphi) & 0 \\ 0 & 0 & 1 \end{bmatrix} \quad (10)$$

$$\mathbf{A}_m = \begin{bmatrix} e_0^2 + e_1^2 - 0.5 & e_1 e_2 - e_0 e_3 & e_1 e_3 + e_0 e_2 \\ e_1 e_2 + e_0 e_3 & e_0^2 + e_1^2 - 0.5 & e_2 e_3 - e_0 e_1 \\ e_1 e_3 - e_0 e_2 & e_2 e_3 + e_0 e_1 & e_0^2 + e_1^2 - 0.5 \end{bmatrix} \quad (11)$$

3 ANALYSIS

The results obtained from the dynamics analysis are presented in figure 6 and 7. Figure 6 shows a comparison of the lateral air gap time-histories according to the presence or absence of the irregular curved guideway, when the Maglev vehicle runs at the speed of 30km/h. In the absence of irregularities, the lateral air gap is controlled around 3mm. But, in the presence of irregularities, the deviation of lateral airgap is within the range of about -9mm to 9mm. it is presumed that the Maglev vehicle negotiate the selected curve, since the deviation of lateral air gap is maintained within an allowable range (nominally 10mm).

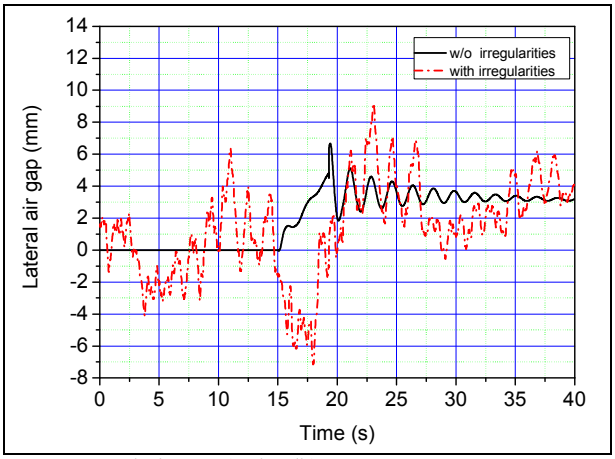

Figure6. Lateral air gap (30km/h)

Figure 7 shows deviation of lateral air gap at 80km/h. The peak value of lateral air gap in the presence of the irregularities is 9mm and in the absence of them is 2mm. Both of two cases are maintained within an allowable range of lateral air gap (nominally 10mm). It is also presumed that the Maglev vehicle negotiate the selected curve.

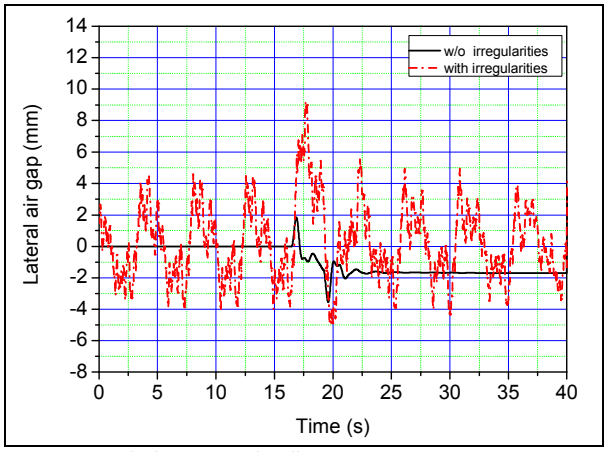

Figure7. Lateral air gap (80km/h)

4 CONCLUSION

In this paper, with the developed model, numerical simulation is performed for the analysis of the dynamic behavior of the vehicle during curving. As lateral air gap plays an important role in curving performance, lateral air gap is measured through the simulation. Consequently, lateral air gap in the two cases of curve are changed within an allowable range at the speed of 30km/h and 80kn/h. Since selected irregularities in simulation are more harshness than them of real guideway, it is presumed that the better curve negotiation will be shown in the actual running test. Furthermore, this simulation could be useful in the prediction of the tolerance of irregularities. Also, design tolerance could be proposed economically when guideway is constructed.

5 REFERENCES

Yim B.H., Han H.S., Lee, J.K., and Kim S.S., Curving performance simulation of an EMS-type Maglev vehicle, *Vehicle System Dynamics*, Vol. 47, No. 10, pp. 1287-1304, 2009.

Lee J.S., Lim D.J., and Kim M.Y., Moving urban Maglev-vehicle analysis considering non- linear magnetic levitational force effect, COSEIK, 2009.

Coenraad E., *Modern railway track second edition*, C. Esveld, Netherlands, 2001.

Shabana A.A., *Railroad vehicle dynamics: A computational approach*, Taylor & Francis Group, USA, 2007.

Yim B.H., and Han H.S., Curve negotiation analysis of a Maglev vehicle utilizing electromagnetic suspension system, Asian Conference on Multibody Dynamics, 2008.

Sinha P.K., *Electromagnetic suspension dynamics & control*, Peter Peregrinus Ltd, London, United Kingdom, 1987.

Han H.S., A study on the dynamic modeling of a magnetic levitation vehicle, *JSME International*, Vol. 46, No. 4, pp. 1497-1501, 2003.